EPJ Web of Conferences **35**, 03004 (2012)
DOI: 10.1051/epjconf/20123503004

Modification of Fe-B based metallic glasses using swift heavy ions

M.D. Rodriguez[1], C. Trautmann[2, 3], M. Toulemonde[4], B. Afra[1], T. Bierschenk[1], R. Giulian[1, a], N. Kirby[5], and P. Kluth[1]

[1]Department of Electronic Materials Engineering, The Australian National University, Canberra, Australia
[2]GSI Helmholtz Centre for Heavy Ion Research, Darmstadt, Germany
[3]Technische Universität Darmstadt, Germany
[4]Centre Interdisciplinaire de Recherche sur les Ions, les Matériaux et la Photonique (CIMAP), Caen, France
[5]Australian Synchrotron, 800 Blackburn Road, Clayton VIC 3168, Australia

Abstract. We report on small-angle x-ray scattering (SAXS) measurements of amorphous $Fe_{80}B_{20}$, $Fe_{85}B_{15}$, $Fe_{81}B_{13.5}Si_{3.5}C_2$, and $Fe_{40}Ni_{40}B_{20}$ metallic alloys irradiated with 11.1 MeV/u ^{132}Xe, ^{152}Sm, ^{197}Au, and 8.2 MeV/u ^{238}U ions. SAXS experiments are nondestructive and give evidence for ion track formation including quantitative information about the size of the track radius. The measurements also indicate a cylindrical track structure with a sharp transition to the undamaged surrounding matrix material. Results are compared with calculations using an inelastic thermal spike model to deduce the critical energy loss for the track formation threshold. The damage recovery of ion tracks produced in $Fe_{80}B_{20}$ by 11.1 MeV/u ^{197}Au ions was studied by means of isochronal annealing yielding an activation energy of 0.4 ± 0.1 eV

1 Introduction

Amorphous metals, also called metallic glasses, are metallic alloys with a disordered non-crystalline atomic structure. The amorphous structure is quenched from the liquid state by rapid cooling with rates of 10^5 to 10^6 K/s. In recent years, these highly processable metallic glasses have attracted a significant degree of both scientific and technological interest due to their interesting physical properties such as high mechanical strength, great wear and corrosion resistance, and high elasticity [1, 2]. The means of tailoring the structurally governed amorphous metal properties have the potential to benefit advanced technological applications.

This research project presents recent results on irradiation effects when exposing amorphous metals to energetic ion beams. When passing through matter, ions with kinetic energy of some MeV per nucleon (MeV/u) lose their energy predominantly via electronic excitation and ionization processes. Energy transfer from the electronic system to the atoms due to electron-phonon coupling may finally melt the material along the ion path. This molten zone rapidly cools down, leading to the formation of long columnar defects along the ion trajectories, so called ion tracks.

The first evidence of ion tracks in metallic glasses was inferred from the observation of the so called "ion hammering" effect occurring at high fluences [3]. Under the bombardment of swift heavy ions, amorphous materials undergo a macroscopic shape change. The sample grows in dimensions perpendicular to the ion beam and shrinks in parallel direction. Microscopic observation of single tracks and analysis of the damage morphology in amorphous materials is challenging due to the lack of sufficient contrast required for most microscopy techniques. Despite this limitation, tracks in metallic glasses were reported using transmission electron microscopy (TEM), including a study of the crystallisation of the material, by means of electron beam annealing [4].

Measurements of ion tracks in amorphous metals were also performed traditionally using the technique of chemical track etching [5], which preferentially dissolves the radiation-damaged track volume at a higher rate than the undamaged bulk material [6]. This destructive process enlarges the nm-sized tracks, erasing the initial damage structure. In addition to track etching, electrical resistivity measurements of irradiated samples were performed. The data allows one to deduce the mean track size from the damage cross section [7], but does not provide any information on the track morphology. To obtain more detailed information about the structure and amorphous state of ion tracks in metallic glasses we thus applied small angle x-ray scattering (SAXS). As demonstrated earlier for a variety of other materials, this nondestructive technique is capable of measuring structural details of ion tracks [8-13] and allows retrieving track radii in

[a] Current address: Instituto de Física, Universidade Federal do Rio Grande do Sul, Porto Alegre, Brazil

amorphous solids with unprecedented precision [10, 11]. Our investigations also include the evolution of track recovery upon annealing using simultaneous SAXS and wide angle x-ray scattering (WAXS) combined with *ex situ* annealing.

2 Experimental

Ribbons of $Fe_{80}B_{20}$, $Fe_{85}B_{15}$, $Fe_{81}B_{13.5}Si_{3.5}C_2$, and $Fe_{40}Ni_{40}B_{20}$ amorphous alloys were irradiated at room temperature under normal incidence with 11.1 MeV/nucleon (MeV/u) ^{132}Xe, ^{152}Sm, ^{197}Au and 8.2 MeV/u ^{238}U ions to fluences between 1×10^{10} and 1×10^{12} ions/cm^2 at the UNILAC accelerator at GSI in Germany. Mass densities and thicknesses of the samples are listed in Table 1.

Table 1. Nominal compositions (in atomic %), mass densities and thicknesses of the reported amorphous metals.

Material	**Mass density** [g/cm^3]	**Thickness** [μm]
$Fe_{80}B_{20}$	7.40	29 ± 1
$Fe_{85}B_{15}$	7.50	15 ± 1
$Fe_{81}B_{13.5}Si_{3.5}C_2$	7.32	29 ± 1
$Fe_{40}Ni_{40}B_{20}$	7.74	26 ± 1

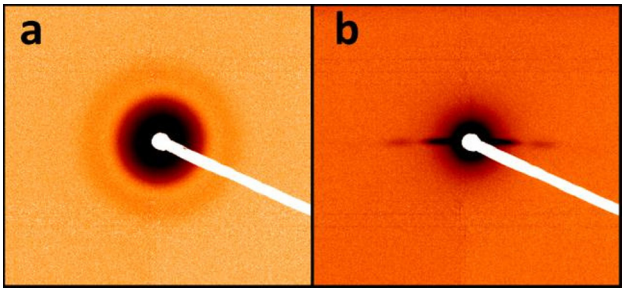

Fig. 1. (Colour online) SAXS images for $Fe_{80}B_{20}$ irradiated with 11.1 MeV/u Au ions at 1×10^{11} ions/cm^2 with tracks aligned at 0° (a) and 10° (b) with respect to the x-ray beam.

The track structure was studied using synchrotron SAXS in transmission mode, performed at the SAXS/WAXS beamline at the Australian Synchrotron. The x-ray wavelength was 1.0332 Å (12 keV) and the distance between the sample and the CCD detector varied between ~1000 and 1600 mm. The samples were mounted on a three-axis goniometer, allowing the precise alignment of the ion tracks with respect to the x-ray beam. Unirradiated samples were used as standards for background subtraction. Measurements as a function of angle between the x-ray beam and the sample surface (i.e. the ion tracks) show a high anisotropy of the scattering pattern (see figure 1) indicating aligned structures of high aspect ratio and giving clear evidence of the existence of ion tracks. This is also consistent with a continuous track morphology and nearly constant energy loss throughout the sample.

To study the annealing kinetics of the ion tracks, we performed isochronal *ex situ* annealing experiments. The SAXS signal of an unirradiated $Fe_{80}B_{20}$ sample and a sample irradiated with 11.1 MeV/u ^{197}Au ions of 1×10^{11} ions/cm^2 was compared as a function of temperature. The annealing of both samples was performed simultaneously, at ambient pressure for 30 min at temperatures between 200 and 450°C. SAXS data were recorded between the different annealing steps.

3 Results and Discussion

3.1 Ion track morphology

The SAXS measurements provide clear evidence of the existence of ion tracks in all alloys tested. Figure 2 shows the experimental scattering intensities originating from an unirradiated sample and from tracks in $Fe_{85}B_{15}$ produced with different ion beams. The SAXS intensities of all tracks exhibit an oscillatory behaviour indicating monodisperse scattering objects with a rather abrupt density change at the track-matrix interface.The SAXS intensities can be well modeled with cylindrical track geometry and assuming constant density in the track, different from that of the matrix material. The scattering intensity can be expressed as $I(q) \sim |f(q)|^2$, where where q is the scattering vector and f the form factor for a cylinder of constant radial density:

$$f(q) = 2\pi LR\rho_0 \, J_1(Rq)/q \qquad (1)$$

L is the track length, R the track radius, ρ_0 the density difference between the track and the matrix material, and J_1 is the Bessel function of first order. To account for deviations from perfectly identical parallel tracks, a narrow Gaussian distribution of the track radii was implemented [10]. The width and position of the oscillations provide the value of the radius R and its polydispersity for the given model, also taking into account the uncertainties of the experimental data in the full q range which are reflected in the uncertainty of the obtained parameters. The solid lines in figure 2 show the fits to the model.

The track radii extracted from SAXS data for $Fe_{85}B_{15}$, $Fe_{80}B_{20}$, $Fe_{81}B_{13.5}Si_{3.5}C_2$ and $Fe_{40}Ni_{40}B_{20}$ amorphous alloys and for existing data on $Fe_{85}B_{15}$ from *in situ* resistivity measurements [7] are shown in figure 3 as a function of the energy loss averaged along the projectile path in the given materials by using the SRIM-2008 code [14]. The error bars in figure 3 represent the depth variation of the track radii associated with the radius polydispersity. It is important to note that the data from reference [7] correspond to irradiation performed at ~90K while our irradiation experiments were performed at room temperature. Smaller track radii are expected at lower irradiation temperatures [10].

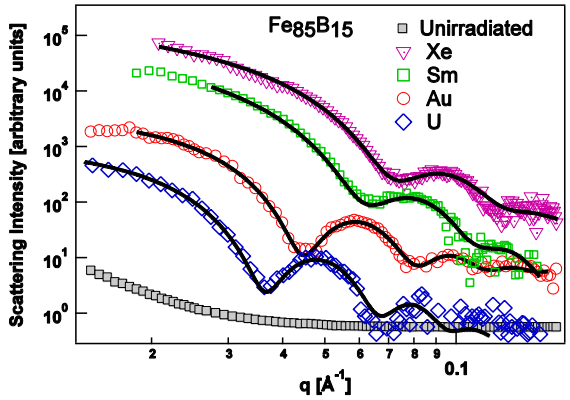

Fig. 2. (Colour online) SAXS intensities (symbols) as a function of scattering vector ***q*** for $Fe_{85}B_{15}$ unirradiated and irradiated with 11.1 MeV/u Xe, Sm, Au, 8.2 MeV/u U ions and cylinder model fits (lines). Scattering intensities for Sm, Au, and U projectiles correspond to 1×10^{11} ions/cm^2 and 3×10^{11} ions/cm^2 for Xe.

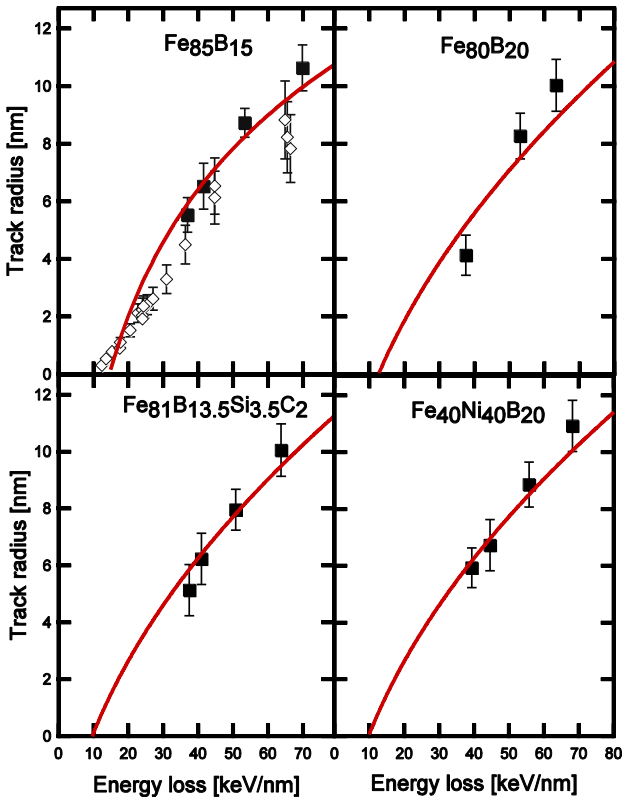

Fig. 3. SAXS track radii (solid symbols) and data deduced from resistivity measurements [7] (open symbols) and i-TS fits (lines) as a function of energy loss.

The good agreement of the SAXS data with a sharp density change at the track boundary is consistent with a molten track that has rapidly been quenched. Melting is the criteria assumed by the inelastic thermal spike model (i-TS) [15, 16] that has been used to successfully describe track formation in the electronic energy loss regime in a variety of materials, including metals [15], amorphous metallic alloys [17], semiconductors [18] and insulators [19]. The i-TS calculations include a superheating scenario during the track formation [9, 20]. The track radii are associated with the cylinder in which the energy deposited on the atoms surpasses the energy E_m necessary to melt the target material along the ion path. Therefore E_m corresponds to the sum of the energy to reach the melting temperature plus the latent heat of fusion. We used this approach to model tracks in amorphous metallic alloys, assuming a constant electron-phonon coupling of 5×10^{12} Wcm^{-3}K^{-1}, deduced by fitting the i-TS model to the track radii measured by SAXS for $Fe_{85}B_{15}$. The energies E_m necessary to melt the different alloys are deduced from the model calculation fits to the SAXS data (see figure 3). The values for E_m and track formation threshold obtained from these calculations are presented in Table 2. From the calculation of the track size versus electronic energy loss, a threshold of 14 ± 2 keV/nm was extracted in good agreement with the value reported in reference [7].

Table 2. Energy required for track melting E_m and track formation threshold S_e deduced from i-TS fits.

Material	**E_m** [eV/at]	**S_e** [keV/nm]
$Fe_{80}B_{20}$	0.58 ± 0.08	13 ± 2
$Fe_{85}B_{15}$	0.60 ± 0.08	14 ± 2
$Fe_{81}B_{13.5}Si_{3.5}C_2$	0.52 ± 0.06	10 ± 2
$Fe_{40}Ni_{40}B_{20}$	0.51 ± 0.06	10 ± 2

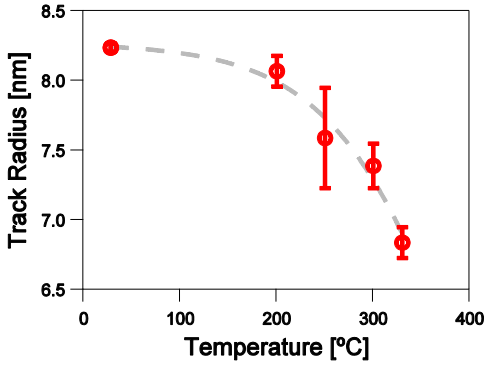

Fig. 4. Track radii deduced from the SAXS data versus annealing temperature for ion tracks in $Fe_{80}B_{20}$ generated with 11.1 MeV/u ^{197}Au ions of 1×10^{11} ions/cm^2. The line is shown to guide the eye.

3.2 Ion track recovery upon annealing

Annealing of irradiated samples leads to a gradual decrease of the track radii due to relaxation at the track boundaries. Figure 4 shows SAXS track radii as a function of annealing temperature obtained for $Fe_{80}B_{20}$ irradiated with 11.1 MeV/u Au ions of 1×10^{11} ions/cm^2.

The activation energy for track recovery was estimated from an Arrhenius plot yielding an activation energy of 0.4 ± 0.1 eV (figure 5). WAXS measurements confirmed that all samples retained their amorphous structure up to 330°C., After the onset of recrystallization at 360°C, no clear SAXS signal from the ion tracks could be detected.

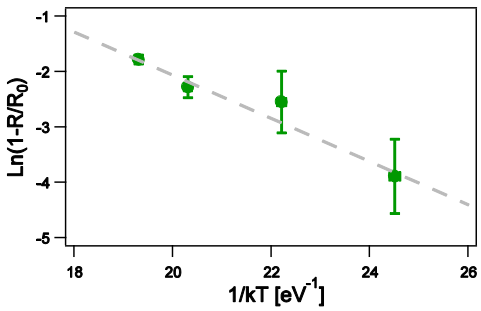

Fig. 5. Arrhenius plot of SAXS track radii in $Fe_{80}B_{20}$ (R_0 corresponds to the track radius at room temperature). From the slope an activation energy of 0.4 ± 0.1 eV for track recovery is deduced

4 Conclusions

Synchrotron SAXS measurements provide evidence for the formation of ion tracks in amorphous $Fe_{80}B_{20}$, $Fe_{85}B_{15}$, $Fe_{81}B_{13.5}Si_{3.5}C_2$, and $Fe_{40}Ni_{40}B_{20}$ ribbons. Depending on the ion species (energy loss), the tracks have a diameter between 6 and 10 nm. Ion tracks in glassy metals can be well described by cylinders of constant density with abrupt boundaries between track and matrix material. According to calculations with the inelastic thermal spike model, the composition of the different Fe-B based alloys has only a minor influence on the track size and critical energy density required for track formation.

Thermal annealing of tracks in $Fe_{80}B_{20}$ generated with 11.1 MeV/u Au ions is characterized by an activation energy of 0.4 ± 0.1 eV. The typical SAXS pattern of tracks vanishes at a temperature close to the onset of recrystallization.

5 Acknowledgements

This research was undertaken on the SAXS/WAXS beamline at the Australian Synchrotron, Victoria, Australia. P.K. acknowledges the Australian Research Council for financial support.

References

1. A. Inoue and A. Takeuchi, Acta Materialia **59**, 2243 (2011)
2. M.D. Demetriou et al., Nature Materials **9**, 123 (2011)
3. M.D. Hou, S. Klaumünzer, G. Schumacher, Phys. Rev. B **41**, 1144 (1990)
4. G. Rizza et al., J. Phys: Cond. Matter **16**, 1547 (2004)
5. C. Trautmann et al., Nucl. Instr. and Meth. In Phys. Res. B **107**, 397, (1996)
6. R. L. Fleischer et al., "Nuclear Tracks in Solids: Principles and Applications", University of California Press, Berkeley (1975)
7. A. Audouard, et al. J. Phys. Condens Matter **5**, 995 (1993)
8. P. Kluth et al., Nucl. Instr. and Meth. In Phys. Res. B **266**, 2994, (2008)
9. P. Kluth et al., Phys. Rev. Lett. **101**, 175503 (2008)
10. M.D. Rodriguez et al., J. Non-Cryst. Solids **358**, 571 (2012)
11. M.D. Rodriguez et al., Microel. Eng. (2012), doi.10.1016/j.mee.2012.05.030
12. B. Afra, et al., Phys. Rev. B **83**, 064116 (2011)
13. B. Afra, et al., Nucl. Instr. and Meth. In Phys. Res. B (2012) dx.doi.org/10.1016/j.nimb.2012.03.007
14. J.F. Ziegler, M.D. Ziegler and J.P. Biersack: http: http://www.SRIM.org
15. A. Dufour, et al., J. Phys. Condens. Matt. **5**, 4573 (1993)
16. M. Toulemonde, , et al., Mater. Res. Soc. Proc. **504**, 99 (1998)
17. M. Toulemonde, et al., Phys. Rev B **46**, 14632 (1992)
18. A. Kamarou, et al., Phys. Rev. B **78**, 054111 (2008)
19. M. Toulemonde, et al., Mat. Fys. Medd. **52**, 263 (2006)
20. M. Toulemonde, et al., Phys. Rev. Lett. **88**, 057602 (2002).